

# Fingerprinting superconductors by disentangling Andreev and quasiparticle currents across tunable tunnel junctions

Petro Maksymovych,<sup>1</sup> Sang Yong Song,<sup>2</sup> Benjamin Lawrie,<sup>2</sup> Wonhee Ko,<sup>3</sup> and Jose L. Lado<sup>4</sup>

<sup>1</sup>*Department of Materials Science and Engineering, Clemson University, Clemson, SC, USA*

<sup>2</sup>*Materials Science and Technology Division, Oak Ridge National Laboratory, Knoxville, TN, USA*

<sup>3</sup>*Department of Physics and Astronomy, University of Tennessee, Knoxville, TN, USA*

<sup>4</sup>*Department of Applied Physics, Aalto University, Espoo, Finland*

(Dated: January 29, 2026)

Tunneling Andreev reflection (TAR) spectroscopy offers a powerful new approach to fingerprint superconducting pairing symmetry at the atomic scale. By leveraging the exponential sensitivity of excess tunneling decay rate to Andreev reflection, TAR robustly distinguishes between s-wave, d-wave, and more complex order parameters, overcoming limitations of traditional conductance-based techniques. Here, using atomistic superconducting transport simulations, we show that the additivity of excess decay rate enables clear separation of Andreev and quasiparticle currents. In particular, we reveal how their competition as well as higher-order scattering processes shape both the decay rate spectra and their dependence on the coupling strength. We show that this phenomenology stems from the fact that Andreev reflection dominates mid-gap conductance for s-wave superconductors, it is suppressed for the d-wave, and it coexists with quasiparticle tunneling in sign-changing symmetries if the expectation value for the superconducting gap remains finite. These distinct spectral fingerprints pave the way for atomically resolved identification of unconventional superconducting states.

## 1. INTRODUCTION

Pairing symmetry provides crucial insights into superconductors [1–4] and can reveal the presence of exotic phenomena like topological superconductivity[5–8]. Many techniques such as muon spin relaxation ( $\mu$ SR) [9, 10], quasiparticle interference imaging [11–14] and point contact Andreev reflection (PCAR) [15–17] have contributed significantly to understanding the symmetry of the order parameter in conventional and unconventional superconductors. However, the definitive assignment remains challenging and often controversial for any new material, stimulating the search for new, complementary, and more direct methods[18–20]. Among them, techniques that exhibit high spatial resolution are particularly useful for addressing the properties of inhomogeneous superconductors and superconducting interfaces enabling creating emerging electronic states [21–28].

Tunneling Andreev Reflection (TAR) provides a new approach to detect Andreev reflection in scanning tunneling microscopy (STM) with near atomic-scale resolution [29, 30]. Whereas traditional point contact Andreev spectroscopy detects excess conductance as a proxy for Andreev reflection across a metal-superconductor junction, TAR is relying on the excess tunneling decay rate ( $\kappa$ ). Methodologically, STM probes tunneling currents at different tunneling couplings ( $\gamma$ ) to precisely measure the coupling dependence of the tunneling current ( $G \sim \gamma^\kappa$ ). Andreev and electron components of the tunneling current can then be disentangled by comparing the exponent  $\kappa$  of the power-law dependence in the superconducting state ( $\kappa$ ) vs normal state ( $\kappa_N$ ). The strong dependency of Andreev reflection current on the tunneling coupling is

well known and is generally considered to be detrimental due to rapid suppression of the excess conductance [16, 17, 31–33]. By contrast, this very same dependency is directly measured in TAR so that this technique can, in principle, operate at arbitrarily small contact transparency.

Understanding the factors that contribute to specific shapes of the  $\kappa$  - spectra in TAR remains an open problem. For the simplest case of an s-wave superconductor, the ratio  $\kappa/\kappa_N$  equals 2 inside the gap. This ratio directly reflects a simple intuitive picture of two particles, an electron and a retroreflected hole, traversing the junction in Andreev reflection [34, 35], with net probability of Andreev reflection being a product of individual tunneling events. However,  $\kappa/\kappa_N$  can readily deviate from 2 [29]. Even for the s-wave,  $\kappa/\kappa_N$  can actually increase beyond 2 at smaller barriers. Meanwhile, for more complicated d, p, and  $s_\pm$  symmetries, the  $\kappa$ -spectra generally exhibit a complex energy dependence [30]. These rich details enable “fingerprinting” superconductors, and ultimately connecting the observations with specific symmetries. It is therefore imperative to establish the fundamental origins of these spectra and further identify signatures of TAR in unconventional superconductors.

Here, we analyze the shape of the  $\kappa$ -spectra representative of several pairing symmetries. The calculated conductance can be decomposed into contributions of Andreev reflection and single quasiparticle tunneling - unlike that measured in the experiments - which is particularly important if several mechanisms can simultaneously contribute to conductance. First, we demonstrate the crucial benefit of  $\kappa/\kappa_N$  - its additivity with respect to contributing conductance mechanisms. We then reveal the basic structural ingredients of the  $\kappa$ -spectra: (1) energy-

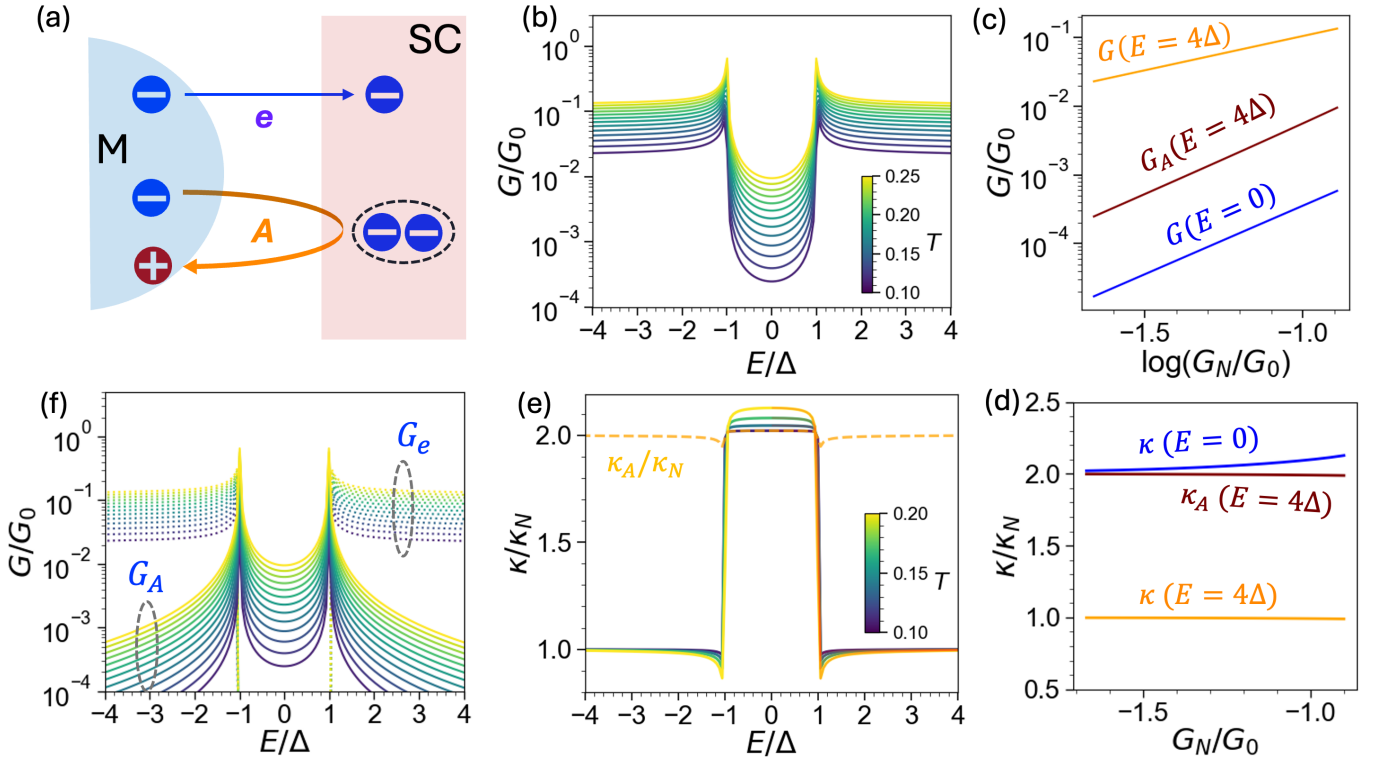


FIG. 1. Simulated conductance and  $\kappa$ -spectra for s-wave superconductor at weak to intermediate coupling strength. (a) Schematic of single quasiparticle tunneling (top) and Andreev reflection (bottom) between a metallic tip and a superconducting sample. (b) Conductance spectroscopy for a range of coupling. (c) Conductance scaling as a function of the normal conductance,  $G_N/G_0$  (measured outside the superconducting gap), for tunneling ( $G_e$ ) and Andreev reflection ( $G_A$ ). (d)  $\kappa/\kappa_N$  calculated for energies inside the gap ( $E = 0$ ), outside the gap ( $E = 4\Delta$ ) and separately for Andreev reflection outside the gap ( $\kappa_A$ ). (e) Excess decay rate ( $\kappa/\kappa_N$ ) spectra calculated from (b). Red highlights spectral reconstruction using Eq. 9 from the main text. Dotted line shows the scaling of only the Andreev reflection channel. (f) Partitioning of the conductance data in (b) into contributions from tunneling (dotted) and Andreev reflection (solid). Colorscales in (b), (d) and (e) follow the values of the coupling strength.  $G_0$  is the conductance quantum.

dependence of Andreev tunneling, particularly for sign-changing and nodal order parameters; (2) the expectation value of the superconducting gap across the Brillouin zone; (3) competition between Andreev and single quasiparticle tunneling in any given junction; and (4) higher order contributions to Andreev reflection that emerge in a narrow window of strong coupling just before collapse of the tunneling barrier. Therefore,  $\kappa$ -spectra will in general reflect both intrinsic properties of the superconductor as well as those of the tunneling transport, providing a wealth of information to characterize complicated materials. It is also now clear that not all features of the  $\kappa$ -spectra will correspond to Andreev reflection, and particular care should be taken when analyzing small excess values of the decay rate.

## METHODS

We model the STM substrate system using a generalized tight binding model of the form

$$\mathcal{H} = \mathcal{H}_{\text{tip}} + \mathcal{H}_{\text{substrate}} + \mathcal{H}_{\text{tunneling}} \quad (1)$$

where we take a normal metal tip with Hamiltonian

$$\mathcal{H}_{\text{tip}} = \sum_{n>0} d_{n,s}^\dagger d_{n,s} \quad (2)$$

where  $d_{i,s}^\dagger$  creates an electron on tip site  $n$  with spin  $s$ . The two-dimensional superconducting substrate Hamiltonian takes the form

$$\mathcal{H}_{\text{substrate}} = \sum_{ijs} t_{ij} c_{i,s}^\dagger c_{j,s} + \sum_{ijss'} \Delta_{ij}^{ss'} c_{i,s}^\dagger c_{j,s'}^\dagger + h.c. \quad (3)$$

where  $c_{i,s}^\dagger$  creates an electron on the substrate site  $i$  with spin  $s$ . We consider a square lattice systems with long range hoppings  $t_{ij}$ , whose specific strengths allows us to create single and multiple Fermi surfaces. The superconducting order  $\Delta_{ij}^{ss'}$  allows us to include both conventional and unconventional superconducting orders within the same model, and specifically s-wave, extended s-wave

and d-wave. The tunable Hamiltonian coupling the tip and substrate takes the form

$$\mathcal{H}_{\text{tunneling}} = \gamma \sum_s c_{0,s}^\dagger d_{0,s} + h.c. \quad (4)$$

The tunneling junction is accounted for by the variable hopping  $\gamma$  connecting metallic tip and superconducting substrate (see schematic in Fig. 1a). From an experimental perspective, the coupling  $\gamma$  shows an exponential dependence as a function of the distance between tip and sample. The tunneling barrier in these calculations is highly localized in space, thereby precluding momentum resolution of tunneling current. This condition approximates STM experiments with atomic-scale contacts [36]. In the tunneling regime, the conductance is proportional to  $T = |\gamma|^2$ , a parameter that we will refer as tip-substrate coupling for the sake of simplicity.

To disentangle the Andreev and quasiparticle contribution, the conductance will be separated into Andreev reflection and single quasiparticle tunneling via decomposition of the scattering matrix into

$$G(\omega, \gamma) = G_e(\omega, \gamma) + G_A(\omega, \gamma) \quad (5)$$

where  $G_e$  corresponds to single electron transmission and  $G_A$  corresponds to double electron transmission, known as Andreev reflection, where an incoming electron gets reflected as a hole. The previous conductances are computed using an  $\mathcal{S}$ -matrix formalism implemented with Nambu non-equilibrium Green's functions [37–41], where the tip is taken as quasi one dimensional and the substrate as an infinite two-dimensional plane. It is worth noting that, although this geometry breaks the translational symmetry of the substrate due to the STM tip, the exact  $\mathcal{S}$ -matrix can be computed using embedded Green's functions [42, 43]. The tunneling dependence of the conductance allows us to define the decay rate as

$$\kappa(\omega, \gamma) = \frac{1}{2} \frac{d \log G(\omega, \gamma)}{d \log \gamma} = \frac{1}{2} \frac{\gamma}{G(\omega, \gamma)} \frac{dG(\omega, \gamma)}{d\gamma} \quad (6)$$

The interpretation of the previous object can be rationalized from the power series of the conductance. The conductance  $G$  will have a dominating power dependence as a function of  $\gamma$  of the form  $G = \alpha\gamma^\beta$  for  $\gamma \ll 1$ . For single electron tunneling, we expect  $\beta = 2$ , whereas for Cooper pair tunneling in a conventional superconductor  $\beta = 4$ . As a result, the decay rate enables one to identify from the tunneling-dependent conductance the presence or absence of Cooper pair tunneling. From Eq. 6 it can be readily observed that the decay rate extracts specifically the power dependence  $\beta$  in the small coupling regime  $\gamma \ll 1$ . In contrast, for stronger coupling regime in  $\gamma$ ,  $\kappa$  enables signaling the presence of higher order power expansions of the conductance. Finally, it is convenient to define the electron and Andreev decay rates as

$$\kappa_T(\omega, \gamma) = \frac{1}{2} \frac{\gamma}{G_e(\omega, \gamma)} \frac{dG_e(\omega, \gamma)}{d\gamma} \quad (7)$$

$$\kappa_A(\omega, \gamma) = \frac{1}{2} \frac{\gamma}{G_A(\omega, \gamma)} \frac{dG_A(\omega, \gamma)}{d\gamma} \quad (8)$$

Specifically, from the definition of Eq. 6, it is straightforward to show that  $\kappa$  is a weighted average of the two contributions:

$$\kappa(\omega, \gamma) = \kappa_T(\omega, \gamma) \frac{G_e(\omega, \gamma)}{G(\omega, \gamma)} + \kappa_A(\omega, \gamma) \frac{G_A(\omega, \gamma)}{G(\omega, \gamma)} \quad (9)$$

where the total conductance  $G = G_e + G_A$  equals the sum of quasiparticle and Andreev conductances (i.e. a parallel circuit). The additive property is a direct consequence of the definition of  $\kappa$  and the additivity of conductance of independent contributing channels. For convenience, in the following we will normalize the decay rates to the decay rate at energies well above the superconducting gap  $\kappa_N$ , which would correspond to single electron transmission.

## 2. RESULTS AND DISCUSSION

We first revisit the simplest case of tunneling into an s-wave superconductor. Fig. 1b presents the variation of the calculated conductance spectrum at  $T = 0$  K as a function of the coupling strength. The largest normal conductance (at  $E = 4\Delta$ ) in Fig. 1b is  $0.13G_0$ , so all the spectra correspond to tunneling regime. Fig. 1c further compares mid-gap (blue) and above-gap (orange) conductance. It is quite evident from these figures that the tunneling conductance grows much faster inside the superconducting gap as a function of increased coupling. The excess decay rate ( $\kappa/\kappa_N$ ) spectra calculated from the conductance spectra are shown in Fig. 1d and e. As we discussed previously [29],  $\kappa/\kappa_N \geq 2$  in the middle of the gap. This spectrum can be calculated at arbitrarily small coupling strength (limited by computational accuracy or noise in the case of the experiment), which is one of the key strengths of the TAR approach. Note that the calculation of  $\kappa(\gamma)$  depends on the coupling between tip and sample  $\gamma$ , and thus can be fundamentally different in the tunneling  $G_N \ll G_0$  and near contact  $G_N \sim G_0$  regimes.

Partitioning the total conductance into contributions due to Andreev reflection ( $G_A$ ) and quasiparticle tunneling ( $G_e$ ), as shown in Fig. 1f, provides a crucial step to understanding the structure of any  $\kappa$ -spectra. For a fully gapped superconductor at 0 K, the quasiparticle current inside the superconducting gap is zero and the conductance is entirely due to Andreev reflection [16, 17]. Meanwhile, outside the superconducting gap the Andreev current (solid lines) coexists with quasiparticle tunneling (dotted lines), (Fig. 1 f), and quickly subsides with increasing energy.

A key property of  $\kappa/\kappa_N$  is its additivity as shown in Eq. 9. Figure 1e overlays  $\kappa/\kappa_N$  calculated using Eq. 9 and

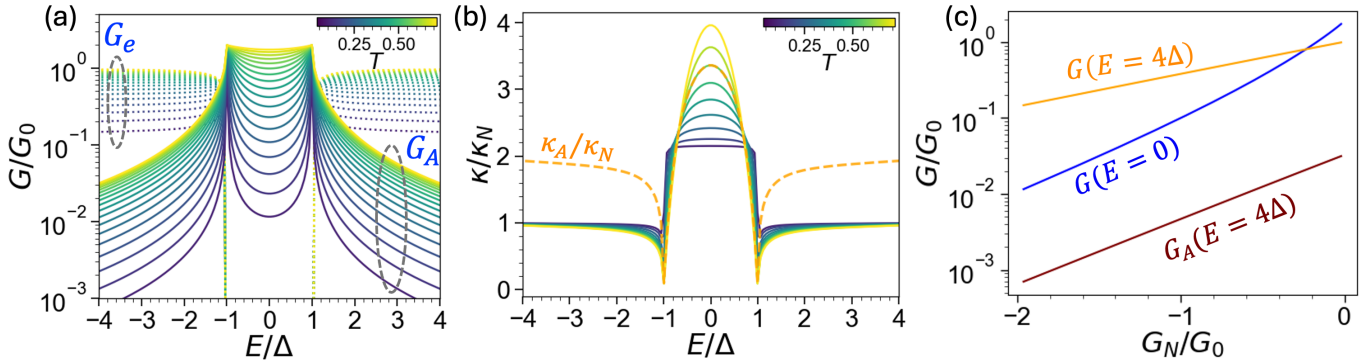


FIG. 2. Near-contact conductance and  $\kappa$ -spectra for s-wave superconductor at strong coupling: (a) Conductance spectroscopy as a function of increasing coupling strength partitioned into contributions from tunneling (dotted) and Andreev reflection (solid). (b) Corresponding  $\kappa/\kappa_N$  spectroscopy. Most notable,  $\kappa/\kappa_N$  significantly exceeds the anticipated value of 2, and can reach as high as 4 as the mid-gap conductance approaches  $2G_0$ . (c) Scaling of the conductance due to tunneling ( $G_e$ ) and Andreev reflection ( $G_A$ ) for several energies as a function of normal conductance (measured outside superconducting gap). Colorscales in (a) and (b) reflect the different tip-substrate coupling strengths  $T = |\gamma|^2$ .  $G_0$  is the conductance quantum.

the Andreev conductance ratio. Clearly, the  $\kappa/\kappa_N$  calculated from separate channels is identical to one calculated from total conductance, which verifies the additivity of the  $\kappa$ . The overall picture at small  $G_N$  is now clear - at 0 K the conductance mechanism is exclusively Andreev reflection inside the superconducting gap. Above the gap energy, Andreev reflection and quasiparticle tunneling coexist. However, the conductance of the Andreev channel is very rapidly suppressed with increasing energy as well as decreasing coupling (compare brown and orange lines in Figure 1c), so that the conductance outside the superconducting gap is almost entirely due to quasiparticle tunneling. As a result, the  $\kappa/\kappa_N$  spectrum is essentially a 1 to 2 transition, with few other significant features in the spectra. One interesting caveat shown in Fig. 1d is that outside the superconducting gap, the excess decay rate due to Andreev tunneling is almost exactly two (brown line), while it is slightly larger than two inside the gap (blue line). We will analyze this property in more detail below.

We now turn to the near-contact regime, where  $G_N$  approaches  $G_0$ . Conductance spectra in this regime begin to rapidly fill the gap (Fig. 2a) due to Andreev reflection (solid lines), and then eventually the mid-gap conductance reaches approximately twice the values outside the gap, a classic signature of Andreev reflection [16, 17]. The  $\kappa$ -spectrum likewise deviates from the weak coupling in this regime. Specifically,  $\kappa/\kappa_N$  can reach values as high as 4 (Fig. 2b) in the window  $G_0 > G_N > 0.1G_0$ . This has been referred as near-contact Andreev reflection [29, 30]. However, as is the case in the weak coupling,  $\kappa_A/\kappa_N$  does not exceed 2, as evidenced by the dashed curve in Fig. 2b and brown line in Fig. 2c, both of which were calculated using only Andreev conductance. Again, using the additivity of  $\kappa/\kappa_N$ , we can rationalize the behavior of the near-contact Andreev reflection. This time,

by allowing multiple reflections in the junction, where for each Andreev reflection, quasiparticles scatter more than twice in the junction region (conceptually similar to Refs. [17, 44]).

To support this statement, we analyze both conductance and unnormalized decay rate ( $\kappa$ ) at several energies as a function of coupling (Fig. 3). As seen in Fig. 3a, the growth of both single quasiparticle tunneling ( $G_e$ ) and Andreev ( $G_A$ ) first exhibit exponential growth at weak coupling, but then the growth rate slows just before the contact. This effect was first reported very early on by Lang [45], and is conceptually explained by the accelerated collapse of the tunneling barrier due to image potential [46]. Correspondingly,  $\kappa$  calculated from the data in Fig. 3a shows this effect quite clearly. The effective tunneling barrier, as well as  $\kappa$ , decrease for any channel with increased coupling, and asymptotically approach zero at contact. Furthermore, decay rate for Andreev reflection above the superconducting gap is nearly exactly twice that of the tunneling. This is easily verified by multiplying the orange function (labeled  $e$ ) in Fig. 3b by 2, and obtaining nearly exactly the brown curve, which itself is calculated numerically from  $G_A$  in Fig. 3a. However, Andreev reflection in the middle of the superconducting gap has a notably different coupling dependence (blue curves in Fig. 3a,b). Although the  $\kappa$  also decreases with increased coupling, it does so first slower than above gap Andreev reflection, and then much faster. This distinct dependency will clearly produce  $\kappa/\kappa_N$  in excess of 2.

We can qualitatively reproduce the behavior of the mid-gap  $\kappa_A$  by constructing a fictitious conductance mechanism,  $G_F = C_1 G_e^2 + C_2 G_e^4$  with two parallel channels and positive coefficients  $C_1$  and  $C_2$ . The fictitious  $\kappa$  (teal dashed curve in Fig. 3b) reproduces the slower decrease of the decay rate, which is similar (though not

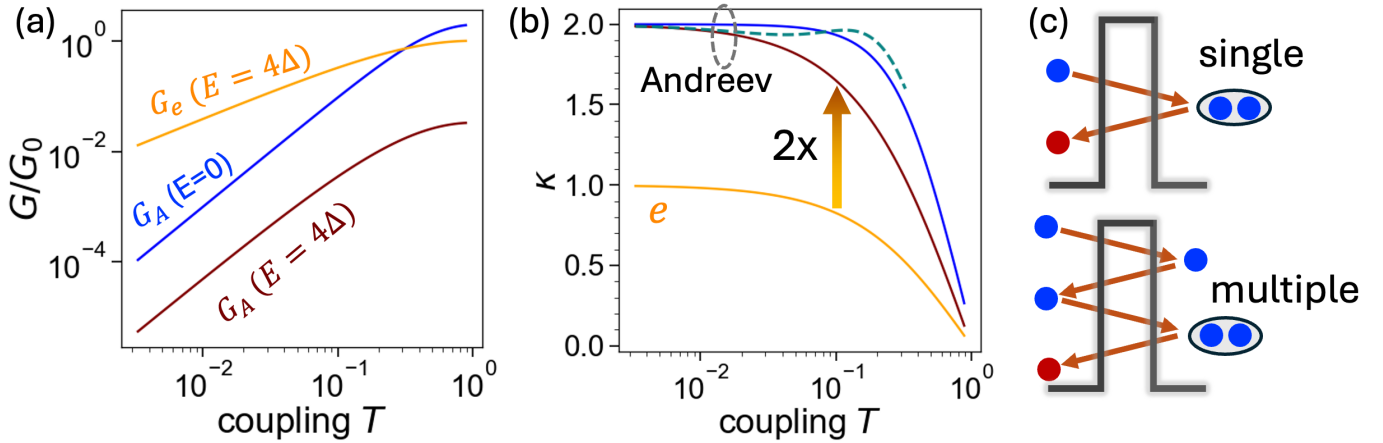


FIG. 3. (a) Conductance for tunneling and Andreev reflection as a function of the tip-substrate coupling strength  $T = \gamma^2$ . The conductance for all channels grows slower when approaching unity coupling due to an effective reduction of the height of the tunneling barrier. The calculated decay rate (b) directly shows this effect for both tunneling (orange) and Andreev reflection (brown). However, the excess decay rate for Andreev reflection is maintained for all coupling strengths. The excess ratio is exactly 2/1 for Andreev reflection beyond the superconducting gap (brown), and is larger than 2/1 for Andreev reflection in the middle of the gap (blue). Larger than 2 ratio can be rationalized by introducing higher order Andreev reflections. For example, the dashed teal line in (b) corresponds to  $\kappa$  calculated from a fictitious conductance mechanism using the formula  $C_1 G_e^2 + C_2 G_e^4$  for Andreev reflection. By construction, this fictitious mechanism is a weighted sum of single and multiple (higher order) Andreev reflections whose schematic trajectories are depicted in (c). The value of the coefficients  $C_1 = 5.5$  and  $C_2 = 11.6$  were determined from least-squares polynomial fit to the blue curve in the conductance range up to  $0.8G_0$ . Although the agreement is only qualitative, the higher order contributions clearly increase the decay rate beyond the excess ratio of 2, similar to the differences between the blue and brown curves in (b)

identical) to the trend of the mid-gap Andreev conductance. The meaning of this new  $G_F$  is also clear - it is a weighted total conductance of the lowest order, single Andreev reflection ( $G_e^2$ ), and a higher order, multiple reflection Andreev process, proportional to  $G_e^4$  (see schematic in Fig. 3c). The existence and increased contribution of the higher order is directly witnessed by the excess decay rate exceeding 2. The higher order scattering should not be confused with multiple Andreev reflection (MAR) in superconducting junction [34, 35, 47]. Instead, it is a single Andreev reflection that proceeds through a sequence of multiple reflections (hence the product of tunneling conductance values), and it naturally arises from the power expansion of the total conductance. The existence of such processes has been proposed several times [17, 44]. However, to our knowledge  $\kappa$ -spectroscopy provides the first direct method to probe them, owing to the additivity of the  $\kappa$  as an observable.

It is worth noting that, while higher-order terms can be observed inside the superconducting gap, outside the superconducting gap their signatures do not manifest even at strong coupling. A simple argument would be that these processes require a minimum of one reflection of a quasiparticle off the superconducting condensate back into the metal lead prior to Andreev reflection (as seen in Fig. 3c). Since there are no propagating states for quasiparticles inside the gap for a fully gapped superconductor, the relative probability of quasiparticle reflection is

high. However, for energies above the gap the large density of propagating states will dramatically reduce the probability of quasiparticle reflection, leaving only single Andreev reflection as a probable process (albeit still with much smaller probability relative to single electron tunneling).

The s-wave analysis above provides the fundamental ingredients needed to interpret the  $\kappa$ -spectra of nodal and sign-changing superconductors. In the following we will discuss  $d_{x^2+y^2}$  and  $s_{\pm}$  pairing symmetry on a Hamiltonian with two Fermi surfaces, previously used to describe FeSe [30]. Figure 4 shows the analysis of  $\kappa$ -spectra for the  $d_{x^2+y^2}$  order parameter with two-Fermi-surface Hamiltonian (Fig. 4a). The conductance and the corresponding  $\kappa/\kappa_N$  spectra are shown in Fig. 4b and c, correspondingly. As we have previously noted, the contrast between s- and d-wave is striking.  $\kappa/\kappa_N$  remains essentially equal to unity across the whole width of the superconducting gap (Fig. 4c). Only in the near-contact regime with  $G_N > 0.1G_0$  the spectra begin to show structure.  $\kappa/\kappa_N$  values grow up to 1.5 in the middle of the gap, and have a pronounced central peak structure that can be qualitatively described as the “inverse” of the gap in the conductance spectra.

It turns out that none of these features correspond to Andreev reflection. The calculated Andreev conductance is negligible compared to tunneling current, as shown in Fig. 4b, for any coupling strength. A complete suppres-

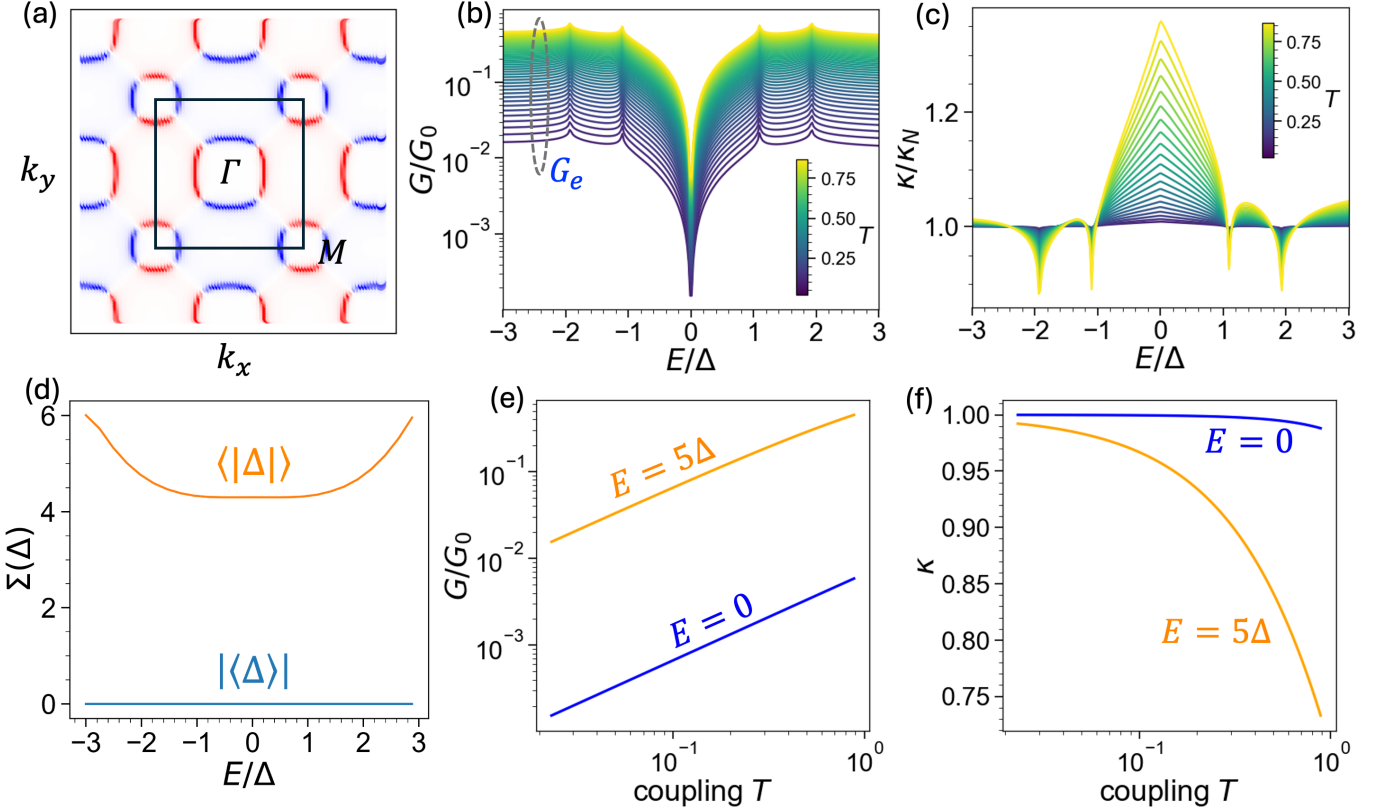


FIG. 4.  $\kappa$ -spectroscopy for a d-wave superconductor, where tunneling Andreev reflection is suppressed: (a) Fermi surface for a two-Fermi-surface electron structure with the d-wave order parameter (b) Conductance spectroscopy as a function of increasing coupling strength. The Andreev contribution to this conductance is below numerical accuracy, so that calculated conductance is from single quasiparticle tunneling at any energy; (c)  $\kappa/\kappa_N$  spectra calculated from conductance in (b). (d) The expectation value of the superconducting gap function ( $\langle|\Delta|\rangle = \int \Delta(\mathbf{k}) d^2\mathbf{k}$ ) across the Brillouin zone is zero at all energies (blue curve), while the average absolute value of the SC gap ( $\langle|\Delta|\rangle = \int |\Delta(\mathbf{k})| d^2\mathbf{k}$ ) remains finite. (e) Conductance and (f) unnormalized decay rate  $\kappa$  as a function of the tip-substrate coupling  $T = |\gamma|^2$ , at energies in the middle ( $E = 0$ ) and outside the ( $E = 5\Delta$ ) the superconducting gap. Mid-gap (blue) conductance saturates slightly slower than outside the gap (orange) when approaching contact, which is effectively captured by the slight differences of the unnormalized  $\kappa$  (e) and  $\kappa/\kappa_N$  spectroscopy (c). Colorscales in (b) and (c) follow the values of the tip-substrate coupling strength  $T = |\gamma|^2$ .

sion of Andreev reflection is rooted in the sign change of the order parameter across the Brillouin zone and an equal volume of the positive and negative gap values. As a result the expectation value of the gap across the Brillouin zone  $\langle\Delta\rangle \equiv \int \Delta(\mathbf{k}) d^2\mathbf{k}$  is zero for any energy (Fig. 4d). It is worth noting that in this situation the average absolute value of the gap  $\langle|\Delta|\rangle \equiv \int |\Delta(\mathbf{k})| d^2\mathbf{k}$  remains finite. The structure of the  $\kappa$ -spectra is then related to the impact of superconductivity in the electronic spectral function, and arises from quasiparticle tunneling. Here too, it is helpful to compare the coupling-dependence of conductance (Fig. 4e) and  $\kappa$  (Fig. 4f) mid-gap (blue) and well outside the gap (orange). The decay rate in the middle of the gap reduces slightly slower with increased coupling. And the  $\kappa$ -spectra sensitively capture this relative difference as a function of energy (Figs. 4c). We propose that this effect is also a signature of higher-order tunneling processes, albeit for single quasiparticle tunneling, and it is rooted in the decrease

of the density of states inside the superconducting gap. In principle this effect should manifest for any electronic gap structure. From the perspective of identifying pairing symmetry, suppression of Andreev reflection in the tunneling junction provides a strong "litmus test" for finite angular momenta Cooper pairing, and in particular d-wave superconductivity, compared to s-wave order parameter, through from a very different perspective than the contact based techniques.

The connection between tunneling Andreev reflection and the average expectation value of the superconducting gap is further strengthened by the analysis of  $\kappa/\kappa_N$  spectroscopy for the  $s_{\pm}$  order parameter (Fig. 5). In our model Hamiltonian (which produces a Fermi surface shown in Fig. 5a), two superconducting gaps are observed, with a completely opened inner gap (Fig. 5b). Unlike Andreev measurements of d-wave superconductors, the Andreev current here persists at all energies and within both gaps for the  $s_{\pm}$  order parameter (Fig. 5b

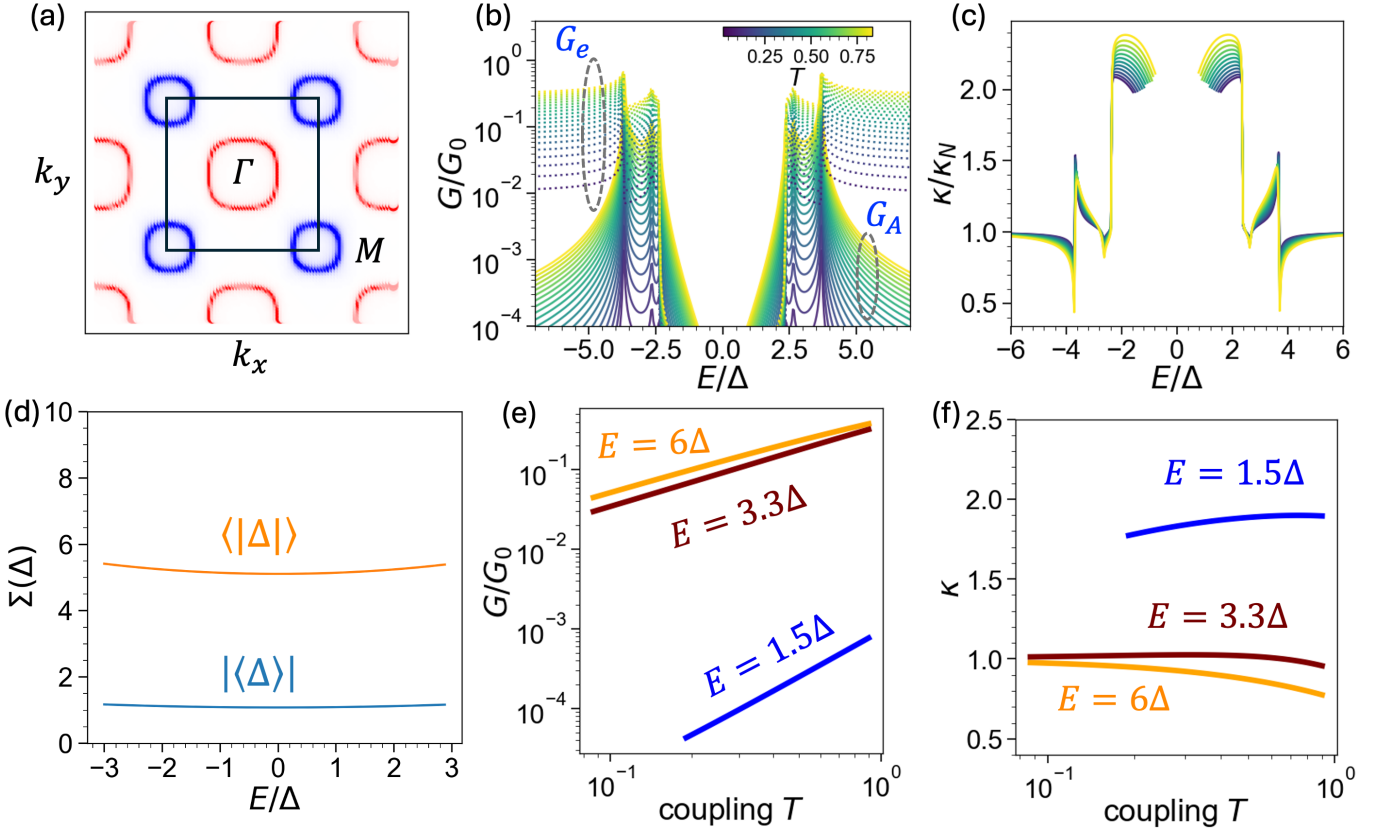


FIG. 5.  $\kappa$ -spectroscopy for  $s_{\pm}$  superconductor, where there exists competition between quasiparticle tunneling and Andreev reflection as a function of energy: (a) Fermi surface of a two-Fermi-surface superconductor with the  $s_{\pm}$  superconducting order parameter. (b) Conductance spectroscopy as a function of increasing coupling strength. Solid lines are the Andreev component ( $G_A$ ), and dotted lines are quasiparticle tunneling ( $G_e$ ); (c)  $\kappa/\kappa_N$  spectra calculated from conductance in (b). (d) Expectation value of both superconducting gap ( $\langle|\Delta|\rangle$ ) and gap magnitude ( $|\langle|\Delta|\rangle|$ ) remain finite at all energies. Scaling of conductance (e) and unnormalized decay rate  $\kappa$  (f) as a function of the tip-substrate coupling  $T = |\gamma^2|$ , at several energies across the gap.

solid curves). As a result, the  $\kappa$  spectrum is now very rich in detail and combines features from both s-wave and d-wave parameters discussed above (Fig. 5c). The persistence of Andreev current is consistent with our hypothesis regarding the expectation value of the superconducting gap. As seen in Fig. 5d, for the chosen parameters, the gap remains finite at all energies. In general, it is of course possible that at some energies for the  $s_{\pm}$  or more complicated order parameters, the gap can become fully compensated, but unlike the d-wave, it is unlikely that complete compensation will be achieved at all energies.

The shape of the  $\kappa/\kappa_N$  spectra can be accounted for by the competition between Andreev and quasiparticle tunneling. The conductance across the inner-most gap is almost exclusively due to Andreev reflection (Fig. 5b,e). Correspondingly,  $\kappa/\kappa_N$  is at and above 2 inside the inner-most gap Fig. 5(c,f). At energies above both superconducting gaps, the Andreev conductance is much smaller than single electron tunneling, so that  $\kappa/\kappa_N = 1$ , similar to the conventional s-wave order. However, at energies between the two superconducting gaps (between approximately  $2.5\Delta$  and  $3.5\Delta$  in Fig. 5(b)), both Andreev and

quasiparticle tunneling can contribute to conductance, particularly with increased coupling. As a result,  $\kappa/\kappa_N$  exhibits a transition from 1 to about 1.5 with increased coupling, and the exact shape of the transition in itself sensitively depends on the specific energy.

Finally, it is worth noting that the additivity of  $\kappa$  enables rationalizing  $\kappa$  spectroscopy at finite temperatures. At a phenomenological level, we can add a linear  $\kappa$ -term to equation (9) weighted by its relative contribution, which will grow with increasing temperature. If normalized by  $\kappa_N$ , this term will just be the conductance ratio of the quasiparticle current due to thermal excitations across the gap. This contribution will be dominant at smaller coupling, but will then compete with Andreev currents at stronger coupling due to the faster growth of Andreev contribution. Specifically, the persistence of Andreev reflection at stronger coupling enabled observing the  $\kappa/\kappa_N$  trace of the superconducting gap in Pb up to the critical temperature [29].

## CONCLUSIONS

We have elucidated the origin and variability of TAR spectroscopy, showing how tunneling Andreev current depends on superconducting gap symmetry and metal-superconductor coupling strength. The likelihood of TAR is governed by the momentum-averaged superconducting gap. For the s-wave symmetry at zero temperature, Andreev reflection solely determines mid-gap conductance; it is entirely suppressed for d-wave order, and for  $s_{\pm}$  symmetry, it remains finite but competes with quasiparticle tunneling as a function of energy. The relative decay rate ( $\kappa/\kappa_N$ ) is additive, allowing all contributions to be rationalized quantitatively in a parallel circuit framework. Notably, as conductance exceeds roughly  $0.1G_0$ , higher-order effects emerge in both Andreev reflection and tunneling, markedly altering the  $\kappa$ -spectra and providing signatures of the superconducting gap even for d-wave symmetry in the absence of TAR. The resulting  $\kappa$ -spectra as a function of STM tip-substrate coupling serve as a distinct fingerprint for each pairing symmetry and electronic structure. Further investigation is needed regarding effects from realistic band structure, multi-channel junctions, topology, and magnetism. Ultimately, the interplay of competing currents and the ability to quantify  $\kappa$ -spectroscopy support its promise for identifying pairing symmetry and exotic quantum states at the atomic scale with TAR.

**Acknowledgments:** (PM) Research was supported by Clemson University. Work at ORNL (BL) was supported by the U.S. Department of Energy, Office of Science, Basic Energy Sciences, Materials Sciences and Engineering Division. J.L.L. acknowledges the computational resources provided by the Aalto Science-IT project and the financial support from InstituteQ, the Finnish Quantum Flagship, the Research Council of Finland (no. 370912), the Finnish Centre of Excellence in Quantum Materials QMAT (no. 374166), and the ERC Consolidator Grant ULTRATWISTROICS (Grant agreement no. 101170477).

---

- [1] C. C. Tsuei and J. R. Kirtley, Pairing symmetry in cuprate superconductors, *Reviews of Modern Physics* **72**, 9691016 (2000).
- [2] A. Chubukov, Pairing mechanism in fe-based superconductors, *Annual Review of Condensed Matter Physics* **3**, 5792 (2012).
- [3] M. Sigrist and K. Ueda, Phenomenological theory of unconventional superconductivity, *Rev. Mod. Phys.* **63**, 239 (1991).
- [4] Z. P. Yin, K. Haule, and G. Kotliar, Spin dynamics and orbital-antiphase pairing symmetry in iron-based superconductors, *Nature Physics* **10**, 845850 (2014).
- [5] K. Flensberg, F. von Oppen, and A. Stern, Engineered

- platforms for topological superconductivity and majorana zero modes, *Nature Reviews Materials* **6**, 944958 (2021).
- [6] X.-L. Qi and S.-C. Zhang, Topological insulators and superconductors, *Rev. Mod. Phys.* **83**, 1057 (2011).
- [7] M. Sato and Y. Ando, Topological superconductors: a review, *Reports on Progress in Physics* **80**, 076501 (2017).
- [8] J. Alicea, New directions in the pursuit of majorana fermions in solid state systems, *Reports on Progress in Physics* **75**, 076501 (2012).
- [9] A. D. Hillier, S. J. Blundell, I. McKenzie, I. Umegaki, L. Shu, J. A. Wright, T. Prokscha, F. Bert, K. Shimomura, A. Berlie, H. Alberto, and I. Watanabe, Muon spin spectroscopy, *Nature Reviews Methods Primers* **2**, 10.1038/s43586-021-00089-0 (2022).
- [10] S. J. Blundell, Muon studies of superconductors, *Annual Review of Condensed Matter Physics* **16**, 367385 (2025).
- [11] F. Ming, X. Wu, C. Chen, K. D. Wang, P. Mai, T. A. Maier, J. Strockoz, J. W. F. Venderbos, C. Gonzlez, J. Ortega, S. Johnston, and H. H. Weitering, Evidence for chiral superconductivity on a silicon surface, *Nature Physics* **19**, 500506 (2023).
- [12] T. Hänke, S. Sykora, R. Schlegel, D. Baumann, L. Harnagea, S. Wurmehl, M. Daghofer, B. Büchner, J. van den Brink, and C. Hess, Probing the unconventional superconducting state of lifeas by quasiparticle interference, *Physical Review Letters* **108**, 10.1103/physrevlett.108.127001 (2012).
- [13] Y. Gao, Y. Wang, T. Zhou, H. Huang, and Q.-H. Wang, Possible pairing symmetry in the fese-based superconductors determined by quasiparticle interference, *Physical Review Letters* **121**, 10.1103/physrevlett.121.267005 (2018).
- [14] S. Wang, K. Zhussupbekov, J. P. Carroll, B. Hu, X. Liu, E. Pangburn, A. Crepieux, C. Pepin, C. Broyles, S. Ran, N. P. Butch, S. Saha, J. Paglione, C. Bena, J. C. S. Davis, and Q. Gu, Odd-parity quasiparticle interference in the superconducting surface state of ute2, *Nature Physics* **21**, 15551562 (2025).
- [15] M. Diez, J. P. Dahlhaus, M. Wimmer, and C. W. J. Beenakker, Andreev reflection from a topological superconductor with chiral symmetry, *Physical Review B* **86**, 10.1103/physrevb.86.094501 (2012).
- [16] G. Deutscher, Andreevsaint-james reflections: A probe of cuprate superconductors, *Reviews of Modern Physics* **77**, 109135 (2005).
- [17] Y. Asano, *Andreev Reflection in Superconducting Junctions* (Springer Singapore, 2021).
- [18] N. Wei, F. von Oppen, and L. I. Glazman, Tunneling spectroscopy of two-dimensional superconductors with the quantum twisting microscope, *arXiv e-prints* , arXiv:2509.22902 (2025), arXiv:2509.22902 [cond-mat.mes-hall].
- [19] M. Khosravian, R. Koch, and J. L. Lado, Hamiltonian learning with real-space impurity tomography in topological moiré superconductors, *Journal of Physics: Materials* **7**, 015012 (2024).
- [20] F. Noronha, A. Canabarro, R. Chaves, and R. G. Pereira, Predicting topological invariants and unconventional superconducting pairing from density of states and machine learning, *Phys. Rev. B* **111**, 014501 (2025).
- [21] T. Shibauchi, T. Hanaguri, and Y. Matsuda, Exotic superconducting states in fese-based materials, *Journal of the Physical Society of Japan* **89**, 102002 (2020).

[22] P. O. Sukhachov, F. von Oppen, and L. I. Glazman, Tunneling spectra of impurity states in unconventional superconductors, *Phys. Rev. B* **108**, 024505 (2023).

[23] E. Liehaber, L. M. Rütten, G. Reecht, J. F. Steiner, S. Rohlf, K. Rossnagel, F. von Oppen, and K. J. Franke, Quantum spins and hybridization in artificially-constructed chains of magnetic adatoms on a superconductor, *Nature Communications* **13**, 10.1038/s41467-022-29879-0 (2022).

[24] L. Schneider, P. Beck, J. Neuhaus-Steinmetz, L. Rzsa, T. Posske, J. Wiebe, and R. Wiesendanger, Precursors of majorana modes and their length-dependent energy oscillations probed at both ends of atomic shiba chains, *Nature Nanotechnology* **17**, 384389 (2022).

[25] L. Jiao, S. Howard, S. Ran, Z. Wang, J. O. Rodriguez, M. Sigrist, Z. Wang, N. P. Butch, and V. Madhavan, Chiral superconductivity in heavy-fermion metal ute2, *Nature* **579**, 523527 (2020).

[26] S. Kezilebieke, M. N. Huda, V. Vao, M. Aapro, S. C. Ganguli, O. J. Silveira, S. Godzik, A. S. Foster, T. Ojanen, and P. Liljeroth, Topological superconductivity in a van der waals heterostructure, *Nature* **588**, 424428 (2020).

[27] D. Huang and J. E. Hoffman, Monolayer fese on srto3, *Annual Review of Condensed Matter Physics* **8**, 311336 (2017).

[28] X. Liu, Y. X. Chong, R. Sharma, and J. C. S. Davis, Discovery of a cooper-pair density wave state in a transition-metal dichalcogenide, *Science* **372**, 14471452 (2021).

[29] W. Ko, J. L. Lado, and P. Maksymovych, Noncontact andreev reflection as a direct probe of superconductivity on the atomic scale, *Nano Letters* **22**, 40424048 (2022).

[30] W. Ko, S. Y. Song, J. Yan, J. L. Lado, and P. Maksymovych, Atomic-scale andreev probe of unconventional superconductivity, *Nano Letters* **23**, 83108318 (2023).

[31] L. Meyer, J. L. Lado, N. Néel, and J. Kröger, Control of andreev reflection via a single-molecule orbital, *Phys. Rev. Lett.* **134**, 146201 (2025).

[32] J. Brand, P. Ribeiro, N. Nel, S. Kirchner, and J. Kröger, Impact of atomic-scale contact geometry on andreev reflection, *Physical Review Letters* **118**, 10.1103/physrevlett.118.107001 (2017).

[33] P. Sukhachov, F. von Oppen, and L. Glazman, Andreev reflection in scanning tunneling spectroscopy of unconventional superconductors, *Physical Review Letters* **130**, 10.1103/physrevlett.130.216002 (2023).

[34] J. C. Cuevas and W. Belzig, Full counting statistics of multiple andreev reflections, *Physical Review Letters* **91**, 10.1103/physrevlett.91.187001 (2003).

[35] G. Johansson, P. Samuelsson, and A. Ingberman, Full counting statistics of multiple andreev reflection, *Phys. Rev. Lett.* **91**, 187002 (2003).

[36] W. Hofer, Challenges and errors: interpreting high resolution images in scanning tunneling microscopy, *Progress in Surface Science* **71**, 147183 (2003).

[37] D. S. Fisher and P. A. Lee, Relation between conductivity and transmission matrix, *Phys. Rev. B* **23**, 6851 (1981).

[38] J. Brand, S. Gozdzik, N. Néel, J. L. Lado, J. Fernández-Rossier, and J. Kröger, Electron and cooper-pair transport across a single magnetic molecule explored with a scanning tunneling microscope, *Phys. Rev. B* **97**, 195429 (2018).

[39] M. P. L. Sancho, J. M. L. Sancho, J. M. L. Sancho, and J. Rubio, Highly convergent schemes for the calculation of bulk and surface green functions, *Journal of Physics F: Metal Physics* **15**, 851858 (1985).

[40] S. Datta, *Electronic Transport in Mesoscopic Systems* (Cambridge University Press, Cambridge, 1995).

[41] J. L. Lado, <https://github.com/joselado/pyqula>.

[42] N. A. García-Martínez, J. L. Lado, D. Jacob, and J. Fernández-Rossier, Anomalous magnetism in hydrogenated graphene, *Phys. Rev. B* **96**, 024403 (2017).

[43] M. Khosravian and J. L. Lado, Impurity-induced excitations in a topological two-dimensional ferromagnet/superconductor van der waals moiré heterostructure, *Phys. Rev. Mater.* **6**, 094010 (2022).

[44] C. W. J. Beenakker, Why does a metal-superconductor junction have a resistance?, in *Quantum Mesoscopic Phenomena and Mesoscopic Devices in Microelectronics* (Springer Netherlands, 2000) p. 5160.

[45] N. D. Lang, Apparent barrier height in scanning tunneling microscopy, *Physical Review B* **37**, 1039510398 (1988).

[46] L. Olesen, M. Brandbyge, M. R. Srensen, K. W. Jacobsen, E. Lgsgaard, I. Stensgaard, and F. Besenbacher, Apparent barrier height in scanning tunneling microscopy revisited, *Physical Review Letters* **76**, 14851488 (1996).

[47] A. W. Kleinsasser, R. E. Miller, W. H. Mallison, and G. B. Arnold, Observation of multiple andreev reflections in superconducting tunnel junctions, *Physical Review Letters* **72**, 17381741 (1994).